

Spanwise coherent structure of wind turbulence and induced pressure on rectangular cylinders

Thai-Hoa Le*

*Department of Engineering Mechanics and Automation, Vietnam National University, Hanoi
144 Xuan Thuy, Cau Giay, Hanoi, Vietnam*

Masaru Matsumoto and Hiromichi Shirato

*Department of Civil and Earth Resources Engineering, Kyoto University
Kyoto-Daigaku-Katsura Campus, Nishikyo-ku, Kyoto 611-8540, Japan*

(Received April 4, 2007, Accepted May 19, 2009)

Abstract. Studying the spatial distribution in coherent fields such as turbulence and turbulence-induced force is important to model and evaluate turbulence-induced forces and response of structures in the turbulent flows. Turbulence field-based coherence function is commonly used for the spatial distribution characteristic of the turbulence-induced forces in the frequency domain so far. This paper will focus to study spectral coherent structure of the turbulence and induced forces in not only the frequency domain using conventional Fourier transform-based coherence, but also temporo-spectral coherence one in the time-frequency plane thanks to wavelet transform-based coherence for better understanding of the turbulence and force coherences and their spatial distributions. Effects of spanwise separations, bluff body flow, flow conditions and Karman vortex on coherent structures of the turbulence and induced pressure, comparison between turbulence and pressure coherences as well as intermittency of the coherent structure in the time-frequency plane will be investigated here. Some new findings are that not only the force coherence is higher than the turbulence coherence, the coherences of turbulence and forces depend on the spanwise separation as previous studies, but also the coherent structures of turbulence and forces relate to the ongoing turbulence flow and bluff body flow, moreover, intermittency in the time domain and low spectral band is considered as the nature of the coherent structure. Simultaneous measurements of the surface pressure and turbulence have been carried out on some typical rectangular cylinders with slenderness ratios $B/D=1$ (without and with splitter plate) and $B/D=5$ under the artificial turbulent flows in the wind tunnel.

Keywords: coherent structure; spanwise coherence; wind turbulence; surface pressure; continuous wavelet transform; wavelet coherence; time-frequency analysis.

1. Introduction

The gust response prediction of structures or long-span bridges immersed in atmospheric turbulence flows subjected to turbulence-induced forces (or buffeting forces) has been based on the strip

* Corresponding Author, E-mail: thle@vnu.edu.vn, thle@arch.t-kougei.ac.jp

theory, by which the spatial distribution characteristic of forces on structure must be taken into account. In the so-called coherent fields such as the turbulence, turbulence-induced pressure and forces, value at a point in these fields is affected by not only this point itself but also other surrounding points. This spatial influence can be generally expressed in either the correlation coefficient function in the time domain or the coherence function in the frequency domain. The spatial correlation or coherence of forces is a key point in theory for the gust response prediction of structures immersed in the turbulence flows. For a sake of simplification, however, the spatial distribution of turbulence field can be used to represent the induced force one. It is usually assumed that, moreover, the spanwise coherence of the induced forces is similar to that of the ongoing turbulence (fluctuating velocity components) that was simplified as an exponential coherence formula in the gust response prediction (Davenport 1963). Recent literatures, however, found out that the coherence of the buffeting forces was larger than that of the ongoing turbulence (Larose 1996, Jakobsen 1997, Kimura, *et al.* 1997, Matsumoto, *et al.* 2003). This suggests that influence of structure on the ongoing turbulence flow must not be negligible, and interaction phenomena between the ongoing flow and the structure might be involved in a modification of the ongoing turbulence flow around the structure (one is mentioned as the bluff body flow). Uncertainty from the force coherence higher than the turbulence coherence can cause either underestimation or overestimation on the gust response prediction of structures. Mechanism of higher force coherence, coherent structures of the turbulence and induced forces as well as effect of the bluff body flow on the force coherence should be further clarified in order to reduce the analytical uncertainty. Coherent structure of the turbulence-induced forces can be generally studied through a mean of surface pressure distribution on model, because induced forces on each model strip can be estimated by an integration of the surface pressure around this strip. Identification of the bluff body flow around structural section (such as the separation bubble, flow reattachment and vortex shedding), furthermore, can be roughly obtained thanks to previous experience and chordwise distribution of mean and fluctuating pressure coefficients which has been verified by means of smoke visualization (Hiller and Cherry 1981, Cherry, *et al.* 1984).

The Fourier transform has been most popularly and conventionally used to study in spectral-based computations, physical data analysis, coherent structures in the frequency domain so far. No time information, however, can be obtained from the Fourier transform-based tools such as the Fourier coefficient, the auto power spectrum, the cross power spectrum, the coherence and phase difference which have been applied to identify the dominant frequency components and the cross correlation between two given time series in the frequency domain. These tools, moreover, are accurately applicable only for purely stationary time series. Wavelet transform has been recently proposed to represent any time series in a time-scale (frequency) plane, known as a time-frequency analysis (Daubechies 1992). First-order wavelet coefficient has mostly been used so far, however, some wavelet transform-based advanced tools corresponding to conventional Fourier transform-based ones such as wavelet power spectrum, wavelet coherence and wavelet phase difference can be developed to express and detect auto, cross correlations of any time series and between two time series in the time-frequency plane (Torrence and Compo 1998, Kareem and Kijewski 2002). The wavelet transform-based tools, furthermore, are advantageous over the Fourier transform as not representing time series in the time-frequency plane but also as a powerful analyzing tool for the non-stationary, non-linear and intermittent time series.

In this paper, the temporal-spectral coherent structures of the wind turbulence and induced pressure will be studied using both the Fourier coherence and the wavelet coherence. Effects of the spanwise separations, bluff body flow and turbulence flow conditions on the coherent structures of

the turbulence and induced pressure, comparison between the wind turbulence and pressure coherences as well as intermittent distribution of the wavelet spectrum and wavelet coherence will be discussed. Physical measurements of the turbulence and induced pressure have been carried out on some typical rectangular cylinders with slenderness ratios B/D=1 (without and with splitter plate at wake region) and B/D=5 under the artificial turbulence flows in the wind tunnel.

2. Fourier transform-based and wavelet transform-based coherences

2.1. Fourier transform-based coherence

The Fourier transform-based coherence is approximately expressed as the normalized correlation coefficient of two spectral quantities of $X(t)$ and $Y(t)$ in the frequency domain (Bendat and Piersol 2000):

$$COH_{XY}^2(f) = \frac{|S_{XY}(f)|}{\sqrt{S_X(f)S_Y(f)}} \quad (1)$$

where $|\cdot|$: absolute operator; f : Fourier frequency variable; $S_X(f)$, $S_Y(f)$, $S_{XY}(f)$: Fourier auto power spectra and Fourier cross power spectrum at/between two separated points, respectively defined as:

$$S_X(f) = E[\hat{X}(f)\hat{X}(f)^{*T}]; S_Y(f) = E[\hat{Y}(f)\hat{Y}(f)^{*T}]; S_{XY}(f) = E[\hat{X}(f)\hat{Y}(f)^{*T}] \quad (2)$$

where $E[\cdot]$: expectation operator; \cdot^* , \cdot^T : complex conjugate and transpose operators; $\hat{X}(f)$, $\hat{Y}(f)$: Fourier transform coefficients of time series $X(t)$, $Y(t)$ respectively. The Fourier coherence is normalized between 0 and 1, thus if two time series $X(t)$, $Y(t)$ are fully-correlated, coherence is unit, whereas coherence is zero if two time series are uncorrelated in the frequency domain.

2.2. Wavelet transform-based coherence

The wavelet transform (also called as continuous wavelet transform) of the given time series $X(t)$ is defined as the convolution operator between $X(t)$ and the wavelet function $\psi_{\tau,s}(t)$:

$$W_X^w(\tau, s) = [X, \psi_{\tau,s}] = \int_{-\infty}^{\infty} X(t) \psi_{\tau,s}^*(t) dt \quad (3)$$

where $W_X^w(s, \tau)$: the wavelet coefficients at translation τ and scale s in the time-scale plane; $[\cdot, \cdot]$ denote the convolution operator; $\psi_{\tau,s}(t)$: wavelet function at translation τ and scale s of the basic wavelet function $\psi(t)$ (the mother wavelet):

$$\psi_{\tau,s}(t) = \frac{1}{\sqrt{s}} \psi\left(\frac{t-\tau}{s}\right) \quad (4)$$

The wavelet coefficients $W_X^w(s, \tau)$ can be considered as a correlation coefficient and a measure of similitude between wavelet and given time series in the time-scale plane. The wavelet scale has its meaning as an inverse of the Fourier frequency, thus inter-relationship between the wavelet scale and the Fourier frequency can be obtained. One would like to develop wavelet transform-based tools such as the

wavelet auto spectra and the wavelet cross spectrum at time shift index i and scale s of two signals $X(t)$ and $Y(t)$, based on their wavelet coefficients $W_{Xi}(s), W_{Yi}(s)$ which are defined with following formulae:

$$WPS_{XXi}(s) = \langle W_{Xi}(s)W_{Xi}^{*T}(s) \rangle; WPS_{YYi}(s) = \langle W_{Yi}(s)W_{Yi}^{*T}(s) \rangle; WPS_{XYi}(s) = \langle W_{Xi}(s)W_{Yi}^{*T}(s) \rangle \tag{5}$$

where $WPS_{XXi}(s), WPS_{YYi}(s)$: wavelet auto spectra of $X(t), Y(t)$; $WPS_{XYi}(s)$: wavelet cross spectrum between $X(t)$ and $Y(t)$; $\langle \rangle$ denotes smoothing operator in both time and scale directions. It is generally noted that the wavelet spectra in Eq.(5) are similar formulations to the Fourier spectra in Eq.(2), the Fourier spectra use the averaging operation in the time domain, but this averaging technique cannot be applied to the wavelet spectra due to presence of the scale and translation parameters, thus it is substituted by so-called smoothing technique in the time and scale domains.

With respect to the Fourier coherence, the squared wavelet coherence of $X(t), Y(t)$ is defined as the absolute value squared of the smoothed wavelet cross spectrum, normalized by the smoothed wavelet auto spectra (Torrence and Compo 1998):

$$WCO_{XYi}^2(s) = \frac{|\langle s^{-1}WCS_{XYi}(s) \rangle|^2}{\langle s^{-1}|WPS_{XXi}(s)| \rangle \langle s^{-1}|WPS_{YYi}(s)| \rangle} \tag{6}$$

where $||$ denotes the absolute operator; s^{-1} is used to convert to an energy density.

The complex Morlet wavelet is the most applicable for physical measurement analysis in the wavelet transform, thanks to its containing of harmonic components and its analogs to the Fourier transform (see Fig. 1):

$$\psi(t) = (2\pi)^{-1/2} \exp(i2\pi f_0 t) \exp(-t^2/2) \tag{7a}$$

$$\hat{\psi}(sf) = (2\pi)^{-1/2} \exp(2\pi^2(sf - f_0)^2) \tag{7b}$$

where f_0, s : central frequency and wavelet scale of the complex Morlet wavelet.

Interrelation between the central frequency, wavelet scale and the Fourier frequency can be determined approximately as follows:

$$f = \frac{f_0 f_s}{s} \tag{8}$$

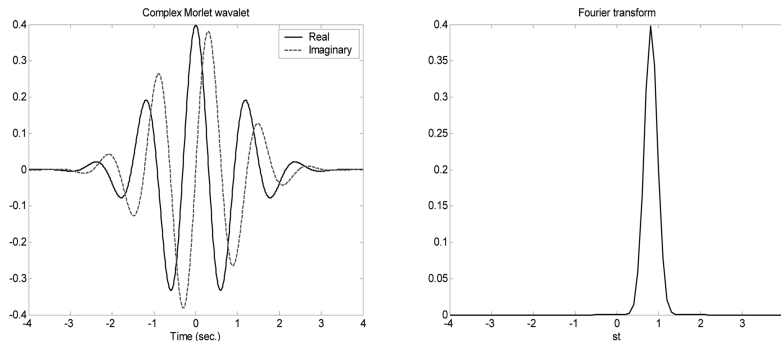


Fig. 1 Complex Morlet wavelet and its Fourier transform

where f_s : sampling frequency of given time series.

Averaging in both time and scale directions is required in the wavelet transform, especially in computing the wavelet spectrum and wavelet coherence. The averaging techniques of the wavelet spectrum in time and scale at the time-shifted index p can be expressed as (Torrence and Compo 1998):

$$\text{Time domain smoothing} \quad \langle WPS_i^2(s) \rangle = 1/N_a \sum_{i=i_1}^{i_2} |WPS_i(s)|^2 \quad (9a)$$

$$\text{Scale domain smoothing} \quad \langle WPS_i^2(s) \rangle = \delta j \delta t / C_\delta \sum_{j=j_1}^{j_2} |WPS_i(s_j)|^2 / s_j \quad (9b)$$

where j assigned between j_1 and j_2 ; N_a : number of averaged points ($N_a = j_2 - j_1 + 1$); δj , δt : factor of window width and sampling period ; C_δ : constant.

Because the wavelet transform deals with finite-length of time series, errors and bias values usually occur at two ends of time series, known as the end effect. One simple solution to eliminate the end effect is to truncate number of discrete results at two ends of time series after the wavelet transform is completed. Removed number, however, depend on the wavelet scale, thus so-called cone of influence should be estimated for more accuracy.

3. Experimental apparatus

Analyzing data were obtained by physical measurements in the Kyoto University's open-circuit wind tunnel. Physical models of the rectangular cylinders with slenderness ratios $B/D=1$ and $B/D=5$ were used, in which model $B/D=1$ was installed without/with the splitter plate (S.P) in the wake of model on account of the effect of wake flow. Motionless models were fixed on a working section. Turbulence flow was generated artificially by grid devices which were located 750 mm upstream from model's leading edge. Wind turbulence and surface pressures were measured in the three turbulence flows at mean wind velocities $U=3, 6$ and 9m/s corresponding to flow case 1, flow case 2 and flow case 3, respectively. Basic turbulence flow parameters were given as turbulence intensities $I_u=11.56\%$, $I_w=11.23\%$ (case 1), $I_u=10.54\%$, $I_w=9.28\%$ (case 2), $I_u=9.52\%$, $I_w=6.65\%$ (case 3). Pressure taps were arranged on one surface of models, consisting of 10 pressure taps on the model $B/D=1$ and 19 pressure taps on the model $B/D=5$ in the chordwise direction (see Fig. 2). Mean and turbulence components (fluctuating velocity ones) of the basic turbulence flow (without model) were measured thanks to a hot-wire anemometer using X-type probes (Model 0252, Kanomax Japan, Inc.) and calibrated and linearized by a constant-temperature anemometer (CTA) (Models 1013, 1011, Kanomax Japan, Inc.). Unsteady surface pressures were measured by multi-channel pressure measurement system (ZOC23, Ohte Giken, Inc.). It is noted that fluctuating velocity components and surface pressures were simultaneously obtained in order to investigate in the time domain. Electric signals were filtered by 100 Hz low-pass filters (E3201, NF Design Block Co., Ltd.) before being passed through the A/D converter (Thinknet DF3422, Pavac Co., Ltd.) with sampling frequency at 1000 Hz in 100 seconds.

Though large number of the pressure taps have been arranged on model surfaces, concretely 10 rows and 21 columns on the model $B/D=1$ (total 210 taps), 19 rows and 41 columns on the model $B/D=5$ (779 taps), but only pressure taps arranged columns at spanwise separations $y=0, 25, 75, 125$ and 225 mm were used in this coherency study (Fig. 2).

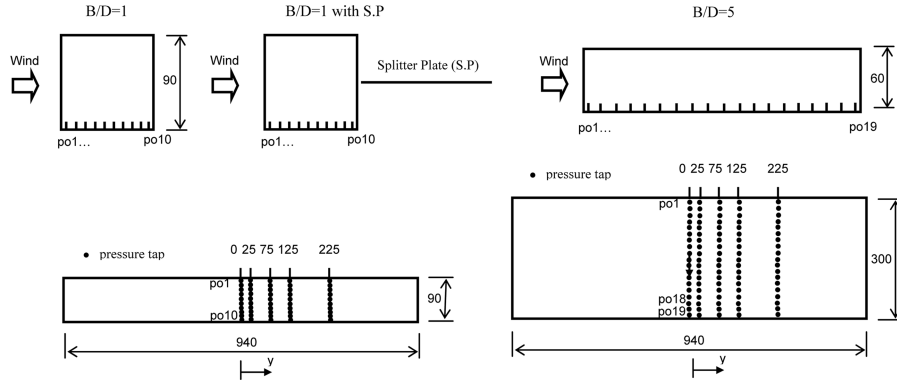


Fig. 2 Experimental models and pressure tap layout

4. Chordwise pressure distribution and bluff body flow pattern

Changed flow around model due to the interaction between original flow and model section is known as the bluff body flow, which characterized by formation of the separated and reattached flows with the separation bubble and that of the vortex shedding as well. It can be predicted from previous studies that the model $B/D=1$ is favorable for dominant formation of Karman vortex shedding in the wake of model, whereas the model $B/D=5$ is typical for formation of the separated and reattached flows on model surface. In case the splitter plate was installed in the wake of the model $B/D=1$, the wake vortex flow and effect of the Karman vortex shedding have been suppressed. Identification of the bluff body flow is usually required for understanding flow behavior and mechanism of oscillation on physical model. The bluff body flow can be identified directly due to flow visualization techniques using smoke, laser sheet, PIV and so on. Pressure distribution is also used for this purpose with experience and knowledge of flow behavior on some typical models. The bluff body flow patterns around the three experimental models can be roughly predicted as shown in Fig. 5.

Normalized mean pressures and normalized root-mean-square fluctuating pressures in the chordwise positions can be determined from measured time series of unsteady pressures as follows:

$$C_{p,mean}^{(i)} = \bar{p}^{(i)} / (0.5\rho U^2); C_{p,rms}^{(i)} = \sigma_p^{(i)} / (0.5\rho U^2) \quad (10)$$

where i : index of pressure time series at chordwise positions; $0.5\rho U^2$: dynamic pressure; \bar{p} : mean value of pressure time series; σ_p : standard deviation of pressure time series.

Fig. 3 shows the normalized mean and fluctuating pressure distributions with respect to the chordwise positions. It can be seen that the normalized mean and fluctuating pressures distribute homogeneously on the models $B/D=1$ without/with the splitter plate, whereas distribute locally near leading edge on the model $B/D=5$. Normalized mean and fluctuating pressures on the model $B/D=1$ without the splitter plate exhibit higher magnitudes than those on the same model but with the splitter plate. Moreover, the normalized mean pressure distributions on the three models seem not to vary with respect to turbulent flow conditions, whereas the fluctuating pressure coefficients increase with an increase of the turbulence intensities.

Auto power spectral densities (PSD) of the fluctuating pressures at some represented positions on the three experimental models in the three flow cases are expressed in Fig. 4. It can be seen with

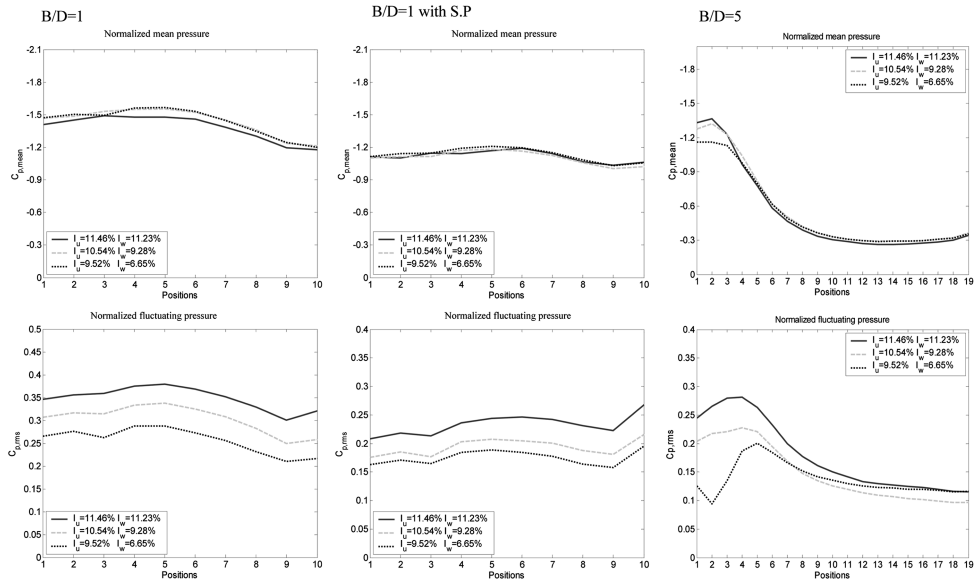


Fig. 3 Normalized mean and fluctuating pressure distributions on chordwise positions

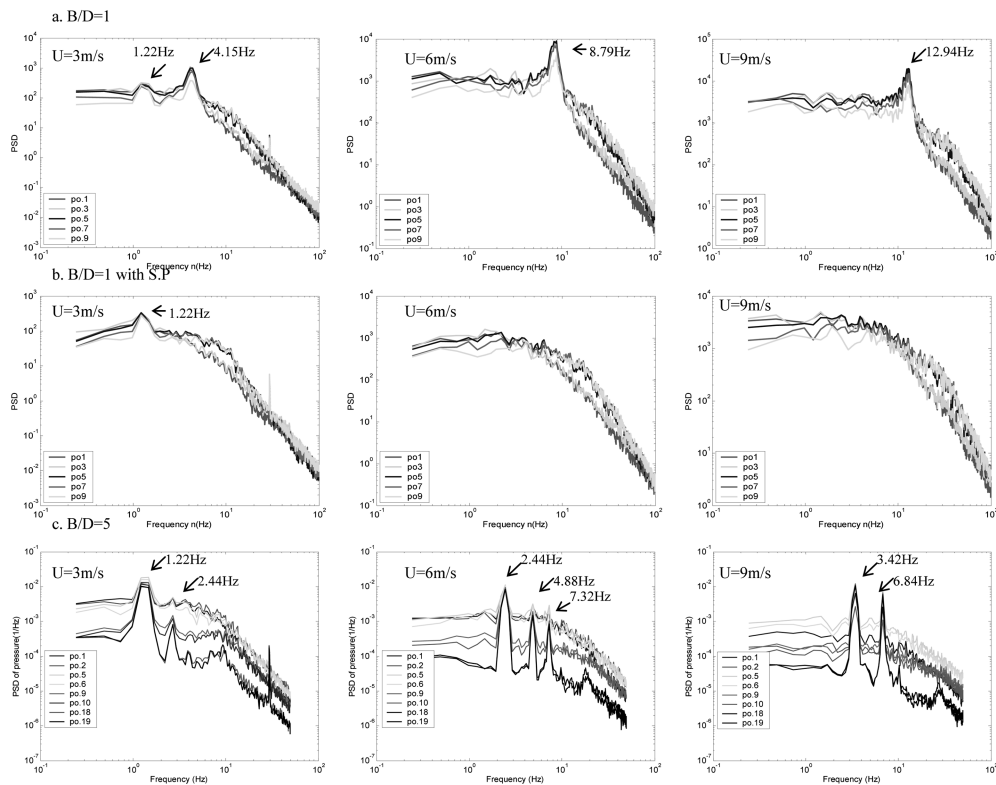


Fig. 4 Auto power spectra of normalized fluctuating pressures at three turbulent flows: a. $B/D=1$, b. $B/D=1$ with splitter plate, c. $B/D=5$

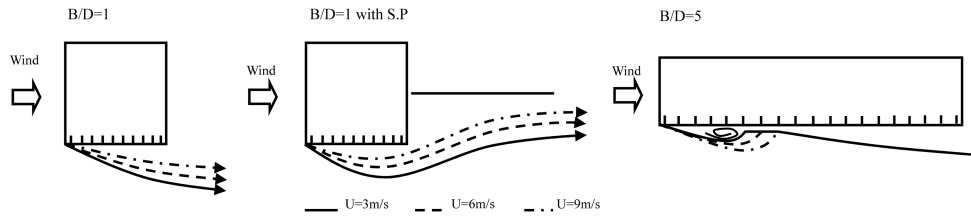


Fig. 5 Bluff body flow patterns around experimental models

the model $B/D=1$ (without the splitter plate) that peaked frequencies are observed at 4.15 Hz, 8.79 Hz and 12.94 Hz respective to the three turbulence flow conditions. It is agreed that the Karman vortex formed and shed in the wake in which the Karman vortex frequency depends on the Strouhal number (St) of model section and mean wind velocity. Moreover, the Strouhal number can be determined as $St=0.1285$. Thus, on the model $B/D=1$ without the splitter plate the bluff body flow is separated at sharp corners, dominated by formation of Karman vortex and frequently shed in the wake. In case of the model $B/D=1$ with the splitter plate, no frequency peaks are observed, this means that the Karman vortex is suppressed by the splitter plate. It is supposed the bluff body flow separated at the sharp corners, this separated flow elongates along the model surface and reattaches at the splitter plate. In case of the model $B/D=5$, frequency peaks are observed at 1.22 Hz and 2.44 Hz (flow case 1); at 2.44 Hz, 4.88 Hz, 7.32 Hz (flow case 2); at 3.42 Hz and 6.84 Hz (flow case 3). According to Hiller and Cherry 1981, Cherry, *et al.* 1984, reattachment point of separated flow may locate just after the position of the peak fluctuating pressure, and the observed frequency peaks are induced by rolled-up turbulent vortices shed away at reattachment points toward trailing edge. Thus, the bluff body flow is separated and reattached on the model surface to form the separation bubble. Reattachment points can be determined at roughly positions 6, 7, 8 with respect to an increase of the mean velocities. High mean and fluctuating pressures are observed locally at the leading edge region in the influence of separation bubble due to local circulation of turbulence eddy inside it.

5. Spectral coherent structure of turbulence and pressure

Effects of the spanwise separations, pressure positions, turbulent flow conditions and Karman vortex on the spectral coherent structures of turbulence and pressure have been investigated using the Fourier coherence. Fig. 6 shows the effect of spanwise separations ($\Delta y = 25, 75, 125, 225$ mm) on the pressure coherence (with all models $B/D=1$, $B/D=1$ with S.P and $B/D=5$) and turbulence coherence on a frequency band $0 \div 100$ Hz and in the flow case 1. It is agreed that the coherences of turbulence and pressure reduce considerably with respect to an increases of the spanwise separations and of observed frequencies.

Coherences of both the turbulence and pressure dominate only at a low frequency band roughly lower than 50 Hz, and they decay fast beyond this frequency. Furthermore, the separation influences on the pressure coherence more than the turbulence one. The turbulence coherence is significant in close separation ($y=25$ mm), but insignificant in other ones ($y=75, 125$ and 225 mm). The pressure coherence, however, suddenly rises even in distant separations at some certain frequencies where any physical phenomenon occurs on the model surface, such as the Karman vortex shedding at the wake and the rolled-up vortex shedding at the reattachment point. Thus, it is discussed that the wind-structure interaction

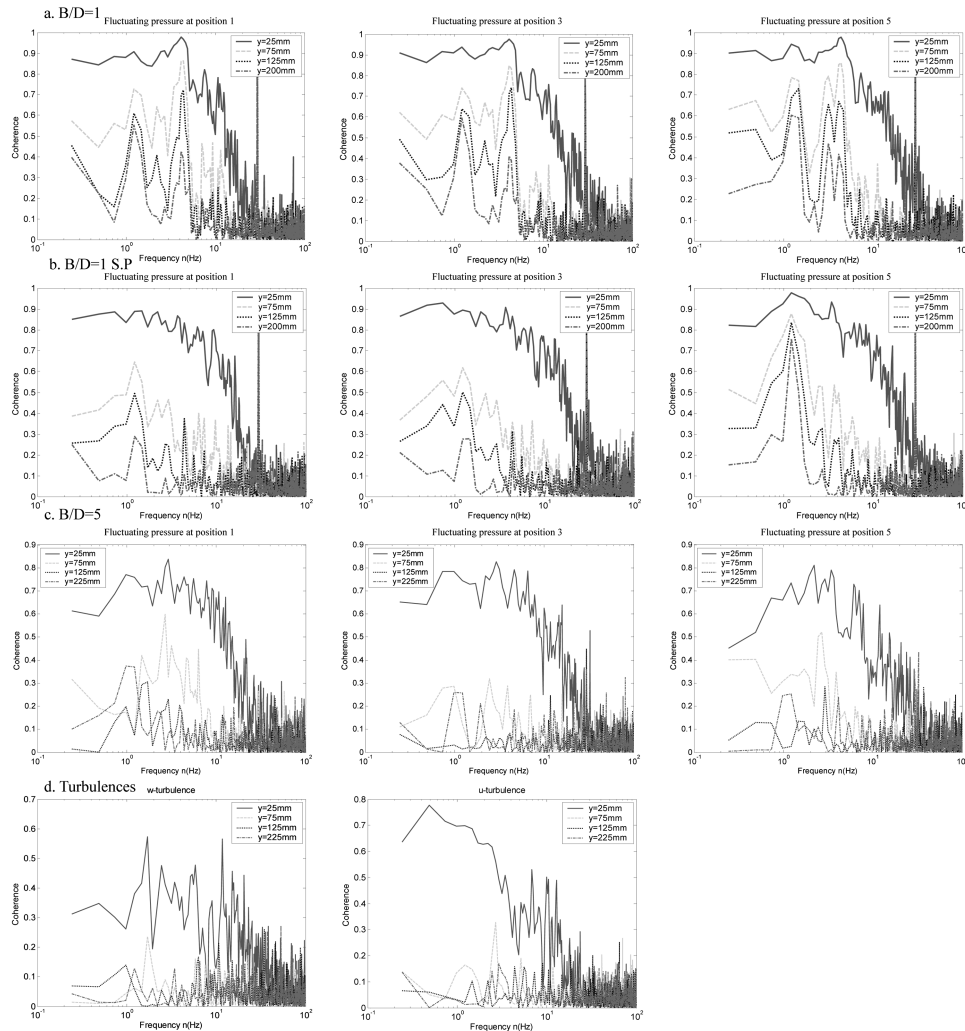


Fig. 6 Effect of spanwise separations on pressure and turbulent coherences in the flow case 1: a. $B/D=1$, b. $B/D=1$ with S.P, c. $B/D=5$, d. turbulences

induces higher pressure coherence than the turbulence one due to enhancing spanwise flow convection.

Fig. 7 shows the pressure coherence at positions Nos. 1, 3, 5, 7, 9 (the models $B/D=1$ without and with S.P) and Nos. 1, 4, 8, 19 (model $B/D=5$) and at the separations ($y=25, 75$ and 125 mm). It can be seen from Fig. 7, the pressure coherences on models $B/D=1$ seem to be not different, except at frequencies of the vortex shedding phenomena, whereas difference in the pressure coherence on the model $B/D=5$ has been observed. In model $B/D=5$, the coherence at position 1 (at the leading edge) seems to be strong in the close separation $y=25$ mm and to be small at the distant separations $y=75, 125$ mm; strong in all separations at the position 4 (in the separation bubble); small in all separations at the position 8 (at the attachment point); and seem to be small in close separation $y=25$ mm and strong in distant separations $y=75, 125$ mm at the position 19 (at the trailing edge) (see Fig. 7c). Thus, it might be supposed that the pressure coherence seems to be relatively high at

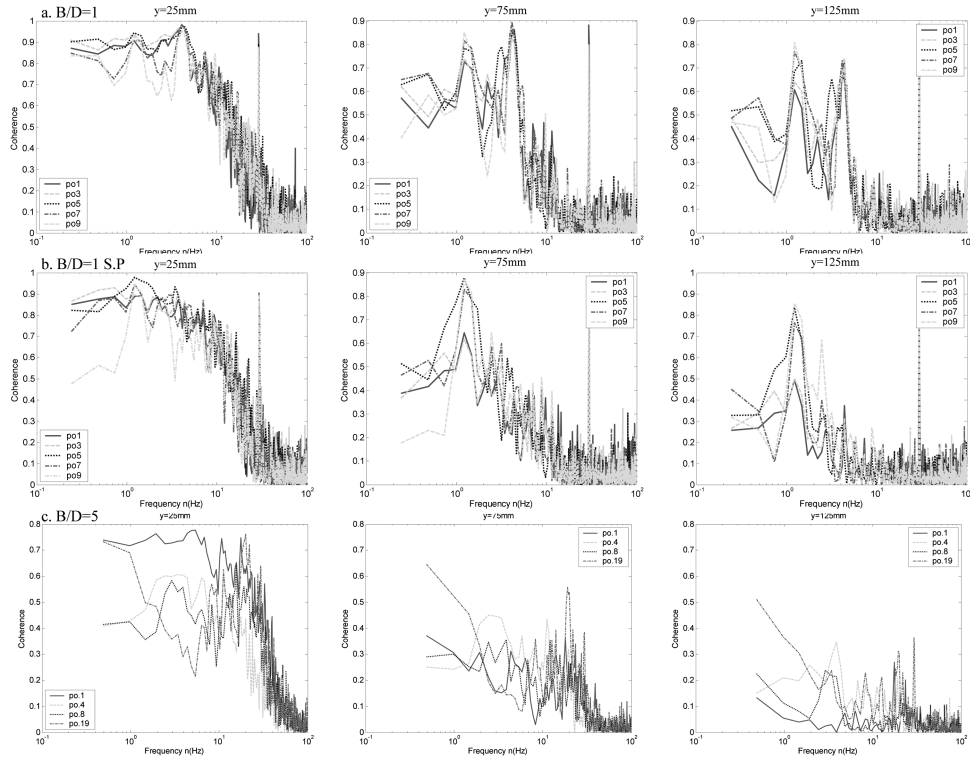


Fig. 7 Effect of pressure positions on pressure coherence: a. $B/D=1$, b. $B/D=1$ with S.P, c. $B/D=5$

the positions in the separation bubble region, to be relatively small at the positions near the reattachment region. Effect of the positions and bluff body flow must be involved for higher mechanism of the pressure coherence.

Effect of the turbulent flow conditions on turbulence and pressure coherences at represented separation $y=25$ mm is presented in Fig. 8. It seems that the pressure and turbulence coherences reduce with an increase of the intensity of turbulence (corresponding to decrease of the mean velocity in turbulence flow). It might be explained that high intensity of turbulence ruins formation of the separation bubble and vortex shedding to resist the spanwise convection of the bluff body flow. Thus, both the turbulent and pressure coherences depend on parameters of the ongoing turbulent flow, not only the mean velocity.

Fig. 9 expresses a comparison between the turbulence and pressure coherences at the spanwise separations $y=25$, 75 and 125 mm, in which the pressure coherences are determined in tap positions 3, 7 at all three experimental models. Obviously, the pressure exhibits higher coherence than the turbulence at the same separations. In the comparison, the coherence of u -turbulence seems to be higher than that of w -turbulence at the close separations $y=25$, 75 mm, but not to be different at the distant one $y=125$ mm. Moreover, the pressure coherences on the three models decrease respectively from the model $B/D=1$ without S.P, $B/D=1$ with S.P to model $B/D=5$. Effect of the Karman vortex shedding on the pressure coherences is more clarified by using the models $B/D=1$ without S.P (formation of the Karman vortex) and with S.P (suppression of the Karman vortex) as seen in Fig. 10. Clearly, the pressure coherence in presence of the Karman vortex is larger than that without the Karman vortex. It implies

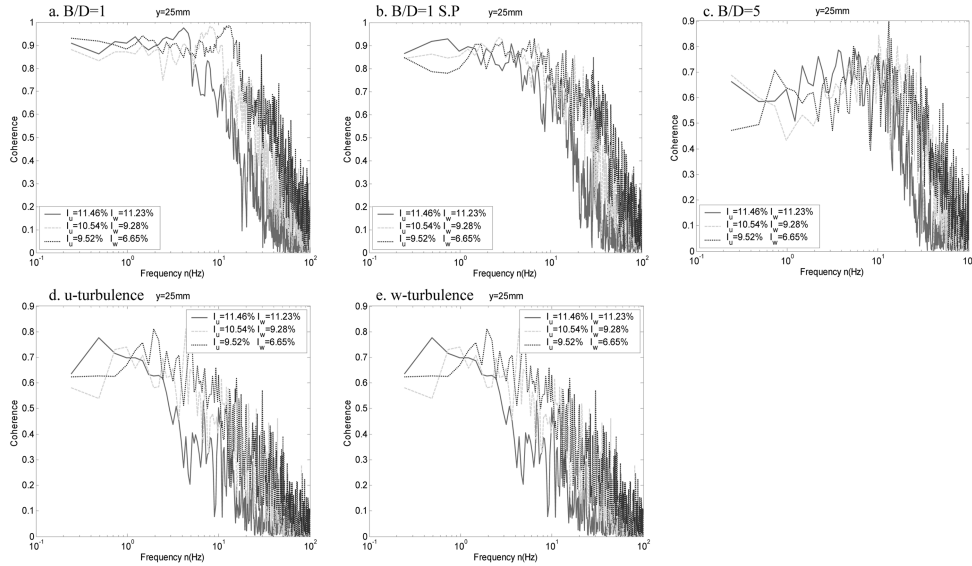


Fig. 8 Effect of turbulent flow conditions of pressure coherence: a. $B/D=1$, b. $B/D=1$ with S.P, c. $B/D=5$, d. u-turbulence, e. w-turbulence

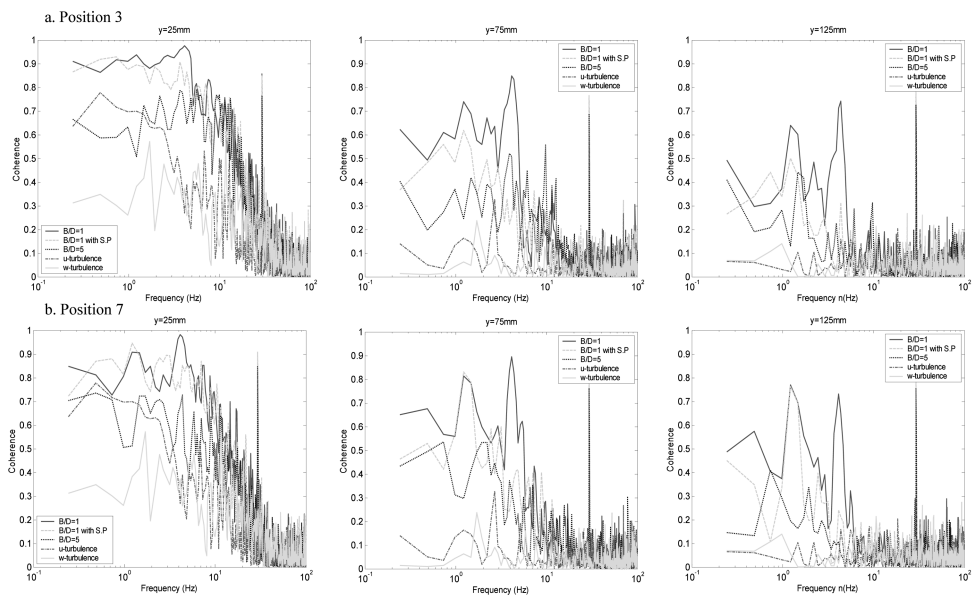


Fig. 9 Comparison between turbulent coherence and pressure coherence: a. at position 3, b. at position 7

that the Karman vortex enhances a spanwise convection of the bluff body flow, and consequently increases the spanwise coherence. In some extent, the slenderness ratio B/D of rectangular sections is a basic parameter to characterize the bluff body flow patterns. It can be generalized that the pressure or force coherences within the influenced spanwise separations reduce with respect to increase of the

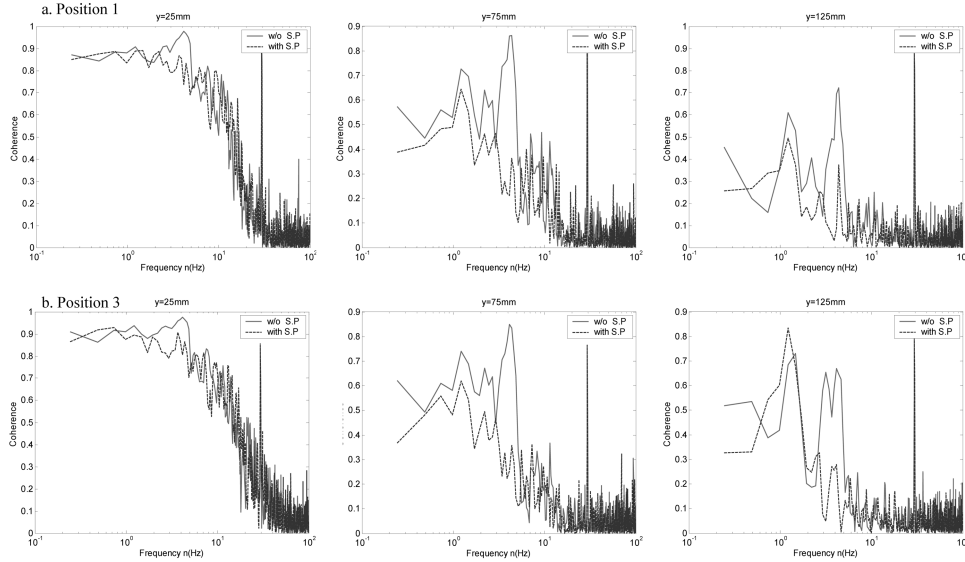


Fig. 10 Effect of Karman vortex shedding on pressure coherence: a. position 1, b. position 3

slenderness ratio B/D and the parameters relating the bluff body flow modification such as the splitter plate at the flow wake, cutting-sharp corners at the trailing edge and so on.

6. Temporo-spectral coherent structure of turbulence and pressure

Temporo-spectral coherent structures of the turbulence and pressure have been studied in the time-frequency plane using the wavelet transform-based tools. The wavelet coefficients, wavelet auto spectra and wavelet cross spectra of the turbulence and pressure have been calculated before the wavelet coherence estimated. Fig. 11 shows the wavelet coherences of the turbulence and pressure corresponding to three experimental models, the separations $y=25, 75$ and 125 mm, on $1 \div 50$ Hz band and $5 \div 95$ second interval.

It can be seen from Fig. 11, some discussions can be given as follows. Firstly, similar to the previous results from the Fourier coherence, the wavelet coherence maps also indicate that the coherence reduces with increase of the spanwise separations, furthermore, the pressure coherences are higher than the turbulence ones at the same separations. However, the coherences of pressure and turbulence are represented in the time-frequency plane in which the coherence is localized and temporo-spectral information determined. Secondly, the coherences of pressure and turbulence are also distributed intermittently and discretely in the time-frequency plane. This implies that the intermittent distributions of turbulence and pressure coherences are observed as the nature of coherence in the time-frequency plane. Thirdly, high coherence events (even to be nearly fully-correlated at some local zones) still exist in both the turbulence and pressure coherences at distant spanwise separations but in localized time-frequency areas. This cannot be clarified from the conventional Fourier coherence and empirical formulae where averaging technique in the time domain has been carried out. Finally, high coherence events of the turbulence and pressure do not correspond in the time-frequency plane, although time series of the pressure and turbulence have

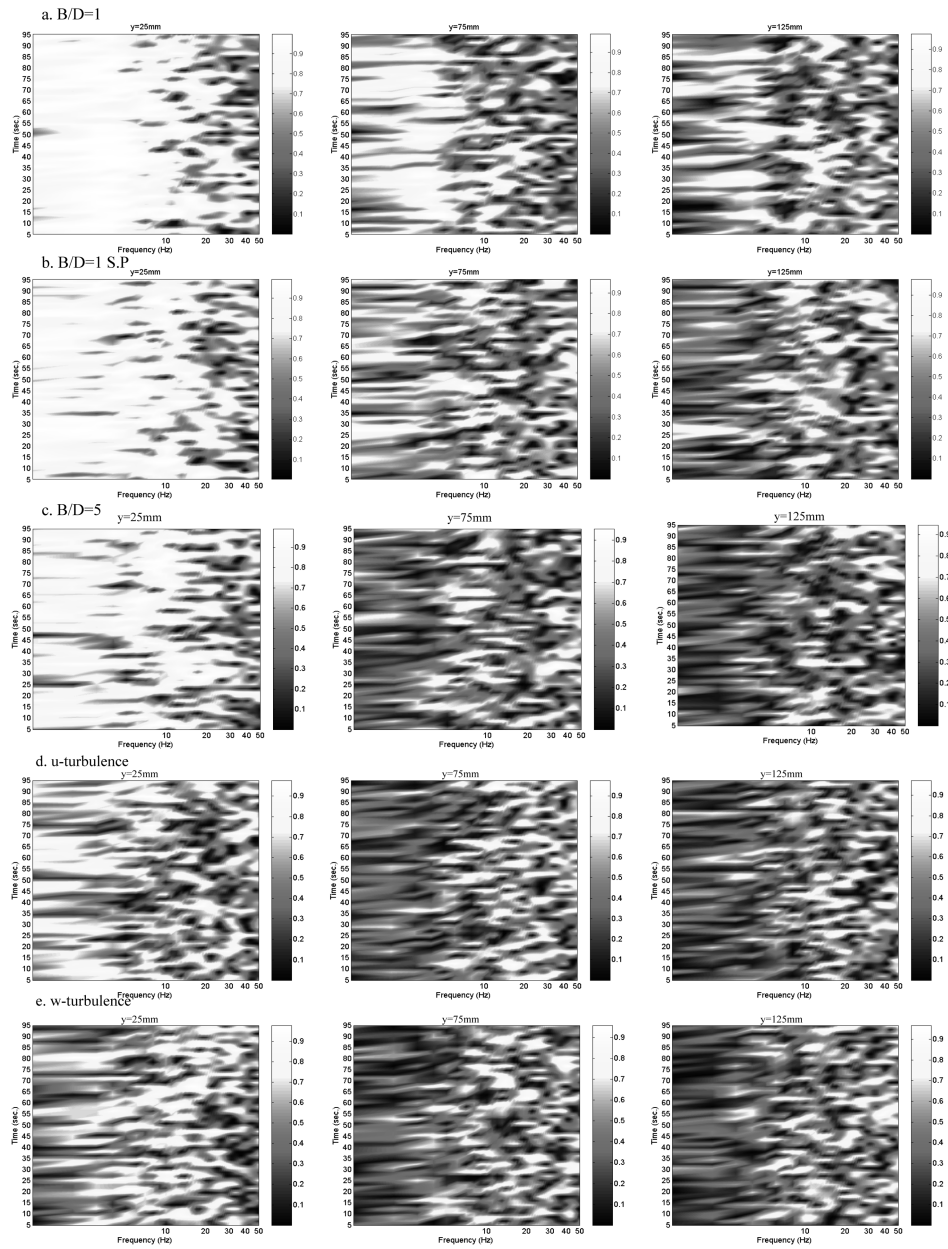


Fig. 11 Wavelet coherence maps of pressure in turbulent flow case 1: a. $B/D=1$, $B/D=1$ with S.P, c. $B/D=5$, d. u-turbulence, e. w-turbulence

been measured simultaneously.

A comparison between the Fourier and wavelet coherences is presented in Fig. 12, in which the pressure coherence on the model $B/D=1$ without S.P and at some spanwise separations is studied. It can be seen from Fig. 12, there is correspondence in dominant spectral components between the wavelet coherence and the Fourier one. The Fourier coherence is appropriate to detect dominant

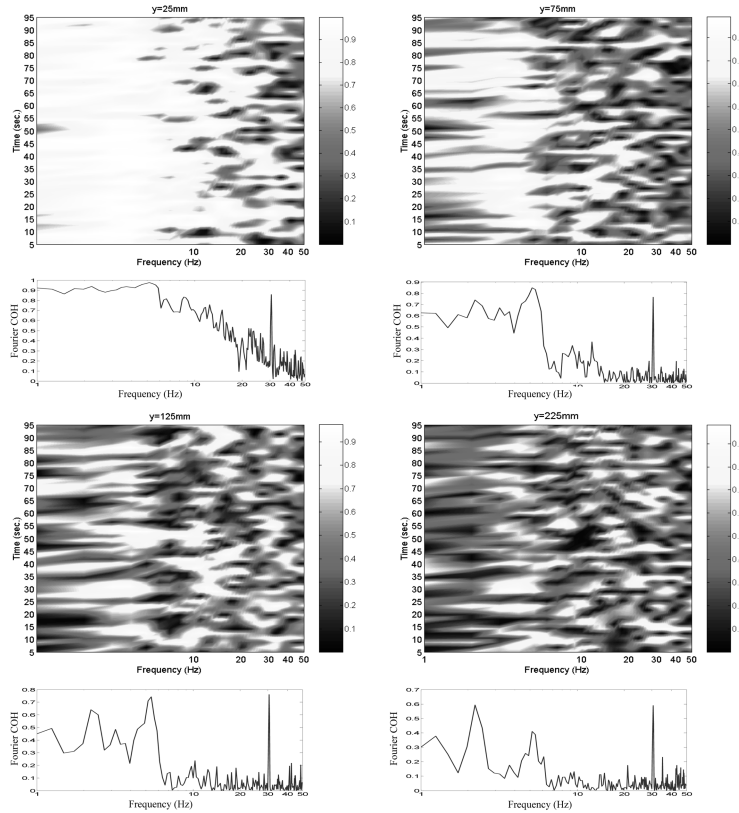


Fig. 12 Comparison between wavelet coherence and Fourier coherence

frequencies of high coherence events, while the wavelet coherence is to track frequency bands of these events. However, there is no time information of the high coherence events obtained at any observed frequencies in the Fourier coherence, but eventual time of those can be given in the wavelet coherence.

7. Conclusion

The coherent structures of turbulence and surface pressure have been discussed in the frequency domain and the time-frequency plane using both the Fourier and wavelet coherences. As discussed above, some conclusions and new findings can be given as follows:

a. The pressure coherence is higher than the turbulence coherence at the influenced spanwise separations. Thus, existing formulae of the force coherence based on the turbulence field might contain an uncertainty.

b. Coherent structures of the turbulence and induced pressure depend on some parameters such as the ongoing flow, spatial separations and bluff body flow. It is reasonable that the empirical formulae for the coherence function of turbulence-induced forces should account for these parameters. Not only the ongoing turbulence flow characteristics (including parameters relating

turbulent flow dimension as turbulent intensities and turbulent scales) and the spanwise separation are accounted in the current coherence formulae, but the effect of bluff body flow should be included in the coherence ones. The slenderness ratio B/D is also suggested as one parameter relating to the bluff body flow in the force coherence for cases of rectangular cylinders.

c. The coherent structures of the turbulence and pressure depend on not only the frequency, but also obviously on the time. Coherence is significant at the low spectral band and distribute intermittently and locally in the time domain. Thus, the intermittency in the time domain and low frequency bands can be considered as the nature of coherent structure.

d. No correspondence and simultaneous occurrence between high coherence events of the turbulence and induced pressure have been observed in the time-frequency plane. This can add to the other uncertainty in the theory of gust response prediction of structures, in which the spatial distribution of the turbulence-induced forces has been assumed similarly as that of the turbulent components.

Acknowledgements

Physical measurements have been carried out at the Structural and Wind Engineering Laboratory, Graduate School of Engineering, Kyoto University under the experimental collaboration with Messrs Kenji Yamane, Takuro Furukawa, Yuya Sumikura to whom the authors would express the many thanks. Authors would like to express the grateful thanks for valuable suggestions of the Reviewers.

References

- Bendat, J.S. and Piersol, A.G. (2000), *Random data: analysis and measurement procedures*, 3rd Edition, John Wiley and Sons.
- Cherry, N.J., Hillier, R. and Latour, M.E.M. (1984), "Unsteady measurements in a separated and reattaching flow", *J. Fluid Mech.*, **144**, 13-46.
- Daubechies, I. (1992), *Ten lectures on wavelets*, Society for Industrial and Applied Mathematics (SIAM).
- Davenport, A.G. (1963), "The response of slender, line-like structures to a gusty wind", *Proc. of Institution of Civil Engineers*, **23**, 389-408.
- Hillier, R. and Cherry, N.J. (1981), "The effects of stream turbulence on separation bubbles", *J. Wind Eng. Ind. Aerod.*, **8**, 49-58.
- Jakobsen, J.B. (1997), "Span-wise structure of lift and overturning moment on a motionless bridge girder", *J. Wind Eng. Ind. Aerod.*, **69-71**, 795-805.
- Kareem, A. and Kijewski, T. (2002), "Time-frequency analysis of wind effects on structures", *J. Wind Eng. Ind. Aerod.*, **90**, 1435-1452.
- Kimura, K., Fujino, Y., Nakato, S. and Tamura, H. (1997), "Characteristics of buffeting forces on plat cylinders", *J. Wind Eng. Ind. Aerod.*, **69-71**, 365-374.
- Larose, G.L. (1996), "The span-wise coherence of wind forces on streamlined bridge decks", *Proc. of the Third International Colloquium on Bluff Body Aerodynamics and Applications*, Blacksburg, USA.
- Matsumoto, M., Shirato, H., Araki, K., Haramura, T. and Hashimoto, T. (2003), "Spanwise coherence characteristics of surface pressure field on 2-D bluff bodies", *J. Wind Eng. Ind. Aerod.*, **91**, 155-163.
- Torrence, C. and Compo, G.P. (1998), "A practical guide to wavelet analysis", *B. Am. Meteorol. Soc.*, **79**(1), 61-78.